


Article

Seismic Reliability Maps of Code-Compliant Italian Reinforced-Concrete Bare and Infilled Frame Buildings

Gianantonio Feltrin, Lorenzo Hofer  and Mariano Angelo Zanini *

Department of Civil, Environmental and Architectural Engineering, University of Padova, Via Marzolo 9, 35131 Padova, Italy; gianantonio.feltrin@phd.unipd.it (G.F.); lorenzo.hofer@unipd.it (L.H.)

* Correspondence: marianoangelo.zanini@unipd.it; Tel.: +39-049-827-5982

Abstract: The present study illustrates the main results of an extensive campaign of numerical simulations aimed at quantifying the seismic reliability of reinforced concrete (RC) bare and masonry-infilled frames compliant with the current Italian Building Code. For this purpose, a set of different residential-use archetype structures are considered, and a prototype seismic design-assessment tool is created to quantify their performance with respect to the relevant limit states, deriving fragility curves via the execution of several non-linear time-history analyses (NLTHAs). The fragilities are subsequently combined with the hazard curves derived for each of the over 8000 Italian municipalities based on the national seismic hazard model currently in force to obtain the respective seismic mean failure rates across Italy. The seismic reliability maps obtained for the investigated code-compliant designs highlight how the current Italian Building Code fails to provide uniform seismic safety across Italy, showing—on the contrary—a strong hazard-dependency. The results are finally used to calibrate regression laws able to correlate the seismic mean failure rates with an intensity measure representative of the seismic hazard.

Keywords: earthquake; seismic design; seismic hazard; structural safety



Citation: Feltrin, G.; Hofer, L.; Zanini, M.A. Seismic Reliability Maps of Code-Compliant Italian Reinforced-Concrete Bare and Infilled Frame Buildings. *Buildings* **2024**, *14*, 1970. <https://doi.org/10.3390/buildings14071970>

Academic Editor: Humberto Varum

Received: 18 April 2024

Revised: 24 May 2024

Accepted: 27 May 2024

Published: 28 June 2024



Copyright: © 2024 by the authors. Licensee MDPI, Basel, Switzerland. This article is an open access article distributed under the terms and conditions of the Creative Commons Attribution (CC BY) license (<https://creativecommons.org/licenses/by/4.0/>).

1. Introduction

Current building codes require structural engineers to design new earthquake-resistant structures able to offer an adequate horizontal capacity with respect to a set of predefined performance levels. Seismic design is commonly performed by practitioners with the classic force-based approach via the use of linear approaches like static analysis or response spectrum analysis, considering the ground motion intensities that have a specified exceedance probability in a given time interval at the building site [1]. For example, seismic design ground motions for ordinary residential-use buildings are derived from the uniform hazard spectrum (UHS), with spectral acceleration values characterized by a 10% in 50 years exceedance probability [2]. Once the action to account for has been defined, designers are asked to fulfill a series of qualitative (e.g., compliance with minimum requirements) and quantitative requirements (i.e., structural checks at the element level, by comparing seismic demands with capacities offered by the sized elements). This approach allows consideration of the uncertainties in only a simplified way (i.e., by setting partial safety factor values that increase actions and decrease material resistances) to avoid the use of complex fully probabilistic analyses [3,4].

However, the sized code-compliant buildings, once assessed, may not show a controlled probability of failure, even if the design ground-shaking intensities are probabilistically defined, as in many codes currently in force worldwide [5,6]. In other words, the use of semi-probabilistic approaches for the seismic design of new buildings is not able to explicitly control the resulting seismic reliability, as investigated for different structural types [7–10]. Code compliance and seismic performance are in fact strictly coupled by a strong underlying relationship, and a modern code must be able to indicate simple

and effective prescriptions that can be implicitly reflected in the fulfilment of the target performance levels a priori defined.

The abovementioned relationship was recently investigated by many studies to quantify the seismic safety and economic losses for different code-compliant building archetypes [11–17]. For example, the Federal Emergency Management Agency (FEMA) in the United States recently published the FEMA P-58-5 Guideline that summarizes the main results of an extended analysis developed to quantify the seismic reliability and risk categories for different code-compliant building types [18]. Some preliminary results were also presented by [19], considering a few building types located in only three sites across Italy, without any clear detail on which level of oversizing the designs were characterized. However, knowledge of the effective spatial distribution of the resulting seismic reliability for code-conforming RC frame buildings in Italy has not yet been analyzed in detail: some recent studies [20,21] tried to address this issue following the approach of Luco et al. [22], considering fragility curves based on the assumption of the median and dispersion values, but not explicitly following a code-compliant seismic design approach like that commonly used by practitioners.

For these reasons, this paper focuses on a more in-depth seismic reliability assessment of code-compliant RC bare and masonry-infilled archetypes to analyze the underlying relationship between seismic design accelerations and the resulting performance in terms of the seismic failure rates, and to compute the Italian seismic reliability maps of such building types. Different configurations are considered in terms of the number of stories (i.e., 3-, 6- and 9-story) as well as the assumed design ductility classes (e.g., high (DCH) and medium (DCM) ductility class). Buildings are automatically designed and later assessed with the use of a prototype seismic design-assessment tool.

This paper is structured as follows. First, the key steps in the prototype seismic design-assessment tool are illustrated, together with a description of the considered archetype structures, showing the main modeling assumptions as well as the results obtained in terms of the fragility curves. Then, the seismic failure rates are computed at the single municipality-level across Italy and illustrated with thematic seismic reliability maps. Lastly, a discussion about the comparability of the results with similar literature studies, the impact of the selected FE modeling approach, the criteria used for the characterization of the hysteresis behavior, and the correlation between the design ground-motion intensities and the resulting seismic reliability is carried out. This discussion will provide some relevant remarks to be addressed when, in the future, the updated version of the Italian Building Code will be released.

2. Seismic Design and Assessment Tool

This section presents a brief description of the prototype seismic design-assessment tool developed by the authors for sizing and subsequently assessing the archetype structures [23]. This tool was developed in a MATLAB environment [24] and linked to a routine in the OpenSees [25] platform for the execution of non-linear time-history analyses (NLTHAs), whose results are post-processed again in MATLAB to compute the related seismic failure rates. In this way, it is possible to design and to assess the seismic vulnerability of code-compliant RC frames for a large number of combinations of floors and spans and for all the possible levels of seismic intensity.

Figures 1 and 2, respectively, show the conceptual flowcharts of both the code-compliant seismic design and the subsequent fragility assessment procedures.

As regards the seismic design procedure, it allows us to design RC frames that are regular in both plan and elevation according to the current Italian Building Code (NTC18). A linear elastic analysis method is considered, and the geometrical and mechanical non-linearities are summarized by the adoption of a proper behavior factor q set on the basis of the assumed ductility class to reproduce the design process that practitioners usually carry out to size such types of buildings.

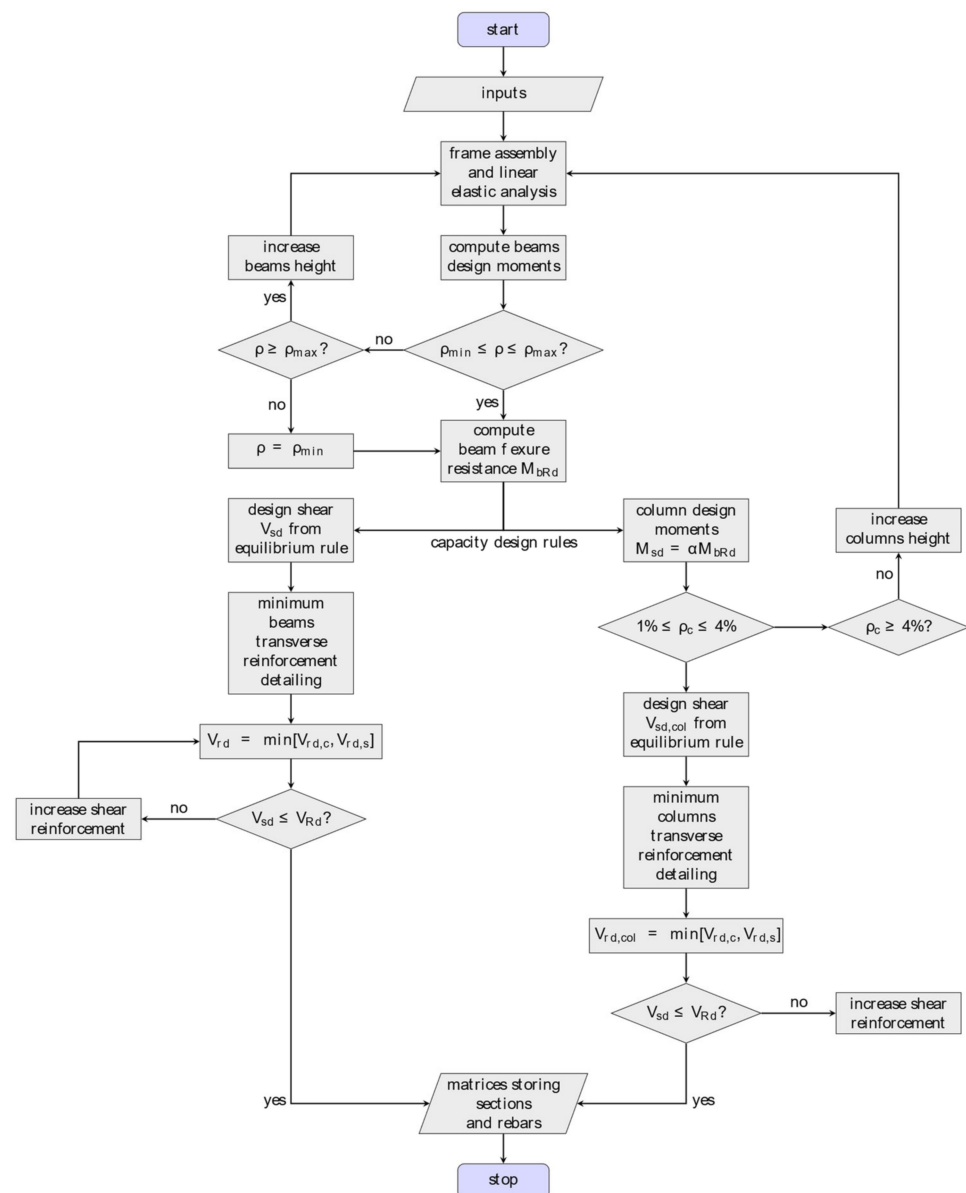


Figure 1. Flowchart of the adopted code-compliant seismic design procedure.

The first step in the procedure consists of the definition of relevant input data, like the number of floors and bays, the first tentative size of the beam sections, the dead load and floor accidental loads unitary values, the elastic uniform hazard spectrum, the desirable ductility class, and the main mechanical characteristics of both the concrete and reinforcing rebars' steel materials. The beam aspect ratio (i.e., height h over width b) is assumed to be higher than 1 to ensure a comparison of results between the DCM and DCH archetypes, given that the choice of wide-shallow beams—where $h/b < 1$ —is currently not allowed by the Italian Code for DCH designs.

The flexural design of the beams is then carried out by first computing the acting bending moments M_{bSd} and thus evaluating the beam longitudinal reinforcement ratio ρ_{lb} required to fulfill the code prescriptions through an iterative loop: if ρ_{lb} is within the lower and upper bound limits (ρ_{min} , ρ_{max}), the flexural capacity M_{bRd} can be computed, whereas if ρ_{lb} exceeds the upper bound limit ρ_{max} , the beam section is modified, increasing height, and the process restarts from the beginning. When the code criterion is met, M_{bRd} is calculated by using the effective amount of longitudinal reinforcement, obtained by finding

the most suitable combination of number of reinforcing rebars and diameter value to be used in relation to the beam section.

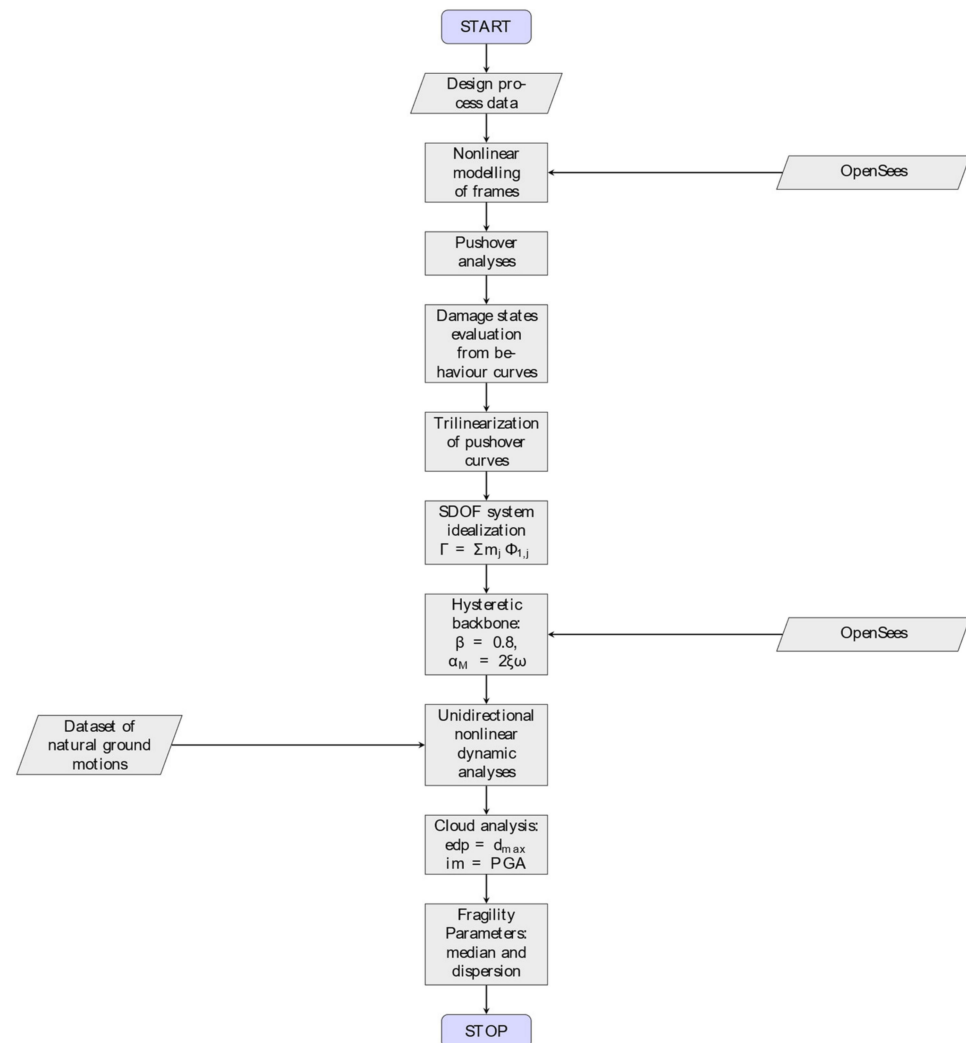


Figure 2. Flowchart of the seismic fragility assessment procedure.

Hence, transverse and longitudinal reinforcement bars, respectively, for beams and columns are computed according to the equilibrium constraints and capacity design rules, as a function of beams' resisting moments M_{bRd} . Namely, the former could be retrieved by imposing the equality of shear actions V_{bSd} with the shear resistance V_{bRd} computed according to the shear resistance model proposed by the Italian Building Code. The columns' flexural design is instead performed by first computing the acting bending moment M_{cSd} by multiplying the beams' resisting moments M_{bRd} by an incremental factor α to comply with the "weak beam–strong column" principle. Even in this case, if the design column longitudinal reinforcement ratio ρ_{lc} exceeds the upper bound limit ρ_{max} , the columns' size would be increased, thus implying the design process to be restarted from the beginning. On the contrary, if ρ_{lc} stands within the lower and upper bound limits (ρ_{min} , ρ_{max}), the procedure allows us to compute the columns' resisting moments M_{cRd} , and in turn, the acting shear demand V_{cSd} via the equilibrium constraints. The last step is to calculate the columns' transverse reinforcement and to account for the code prescriptions in terms of the reinforcement detailing to ensure the achievement of the desired ductility class. Hence, all the seismic rules provided by the Code have been satisfied and the developed procedure guarantees the ductile behavior of the size frames.

Design outputs like the geometrical characteristics of the beams and columns sections, as well as the number of reinforcement bars and diameters, are stored in matrices to be further used as new inputs for the automatic generation of the non-linear numerical model to be used in the seismic fragility assessment procedure. The results of the developed designing tool were also validated by comparing them with those obtained with commercial software.

This procedure has been used for automatically sizing both the bare and infilled RC frame configurations, given that considering a code-compliant design perspective, in the current Italian Building Code it is not mandatory to explicitly consider infills as structural members, but they are often only embedded in the numerical model as additional masses by practitioners.

Once designed, the code-compliant frames are assessed for the relevant performance levels to quantify the related fragility curves, as shown in Figure 2. To accomplish this, a further seismic fragility assessment procedure has been implemented. As a first step, the outputs of the seismic design procedure are used as input data to build the Multi-Degree of Freedom (MDOF) numerical non-linear model of the frames in OpenSees environment. These means that a proper script has been developed in order to assemble the numerical model, starting from the outcomes stored at the end of the design process.

A lumped plasticity modeling technique with plastic hinges calibrated via a fiber cross-section discretization modeling strategy with non-linear stress–strain material laws is adopted. The elements' and joints' shear failure mechanisms are neglected since the fulfilment of the code prescriptions (i.e., the capacity design rule) implicitly avoids their occurrence. For this reason, the adopted modeling strategy aims to represent the flexural behavior of the RC frames. The masonry infills are modeled with equivalent struts in order to capture the increase in stiffness of the structure considered as a whole, as caused by the interaction of the masonry panels with the RC frame.

The procedure starts computing the capacity curve of the frame with a pushover analysis. The frame is then idealized as an equivalent Single Degree of Freedom System (SDOF). The hysteretic behavior of the equivalent SDOF model is characterized by a first elastic branch, a second perfectly plastic behavior and a final decreasing linear post-capping fitted over the pushover results, which is further divided by the modal participation factor of the first mode Γ . The criteria followed for the derivation of the idealized tri-linear capacity curve, as well as the definition of the hysteretic material model used to simulate the cyclic response of the equivalent SDOFs, are reported in detail in [26]. NLTHAs are then directly performed on the equivalent SDOF model to reduce the computational burden and obtain samples of the non-linear seismic behavior of the frame. The NLTHA results are further processed with the Cloud Analysis method since, among others proposed in the scientific literature, it shows the highest effectiveness and flexibility for such a type of analysis. In detail, equivalent SDOF systems are subject to a set of n unscaled ground motion records and the fragility curve takes its origin from the sample of n ground motion intensities and the corresponding sample of structural responses by looking at a suitable engineering demand parameter (edp) able to suitably describe the structural damage, with the following expressions:

$$P[f|im] = P[EDP > \overline{edp}|im] = 1 - P[EDP \leq \overline{edp}|im] = 1 - \Phi \left[\frac{\ln(\overline{edp}) - \ln(edp)}{\beta} \right] \quad (1)$$

$$\ln(\theta) = \ln(a) + b \cdot \ln(im) \quad \sigma = \sqrt{\frac{\sum_{i=1}^{N_{GM}} [\ln(edp_i) - \ln(\theta)]^2}{N_{GM} - 2}} \quad (2)$$

where \overline{edp} represents the specific threshold level of the edp , $\ln(edp)$ is the estimate of the median demand obtained via a liner regression in the bi-logarithmic space, N_{GM} is the sample of ground motion intensities im , β is the demand logarithmic standard deviation and Φ is the standard normal cumulative density function.

Hence, the seismic failure rate λ_f is computed as follows:

$$\lambda_f = \int_{im} P[f|im] \cdot |d\lambda_{im}| \quad (3)$$

where λ_{im} is the seismic hazard curve representative of the seismicity at the site of interest, usually quantified via a Probabilistic Seismic Hazard Analysis [27,28], im is a relevant ground-shaking intensity measure, and $|d\lambda_{im}|$ stands for the absolute value of the differential of the hazard curve.

3. Archetype Structures

This paper investigates the seismic reliability of code-compliant residential buildings with an RC frame-resisting scheme. Figure 3 illustrates the main features of the different configurations analyzed, which fulfill the plan and elevation regularity criteria and are characterized by three increasing elevations, i.e., 3-, 6- and 9-story archetypes, all with a constant inter-story height equal to 3 m. All the configurations have a rectangular plan with 5×3 bays of 5 m span each and wants. The considered structural archetypes want to reasonably represent the structural behavior of the vast majority of the new buildings designed meeting the regularity criteria suggested by the current building code [29]. Note that old buildings or those built with different standards with respect to the current building code or different design loads and/or materials might not be represented by the analysis in this work.

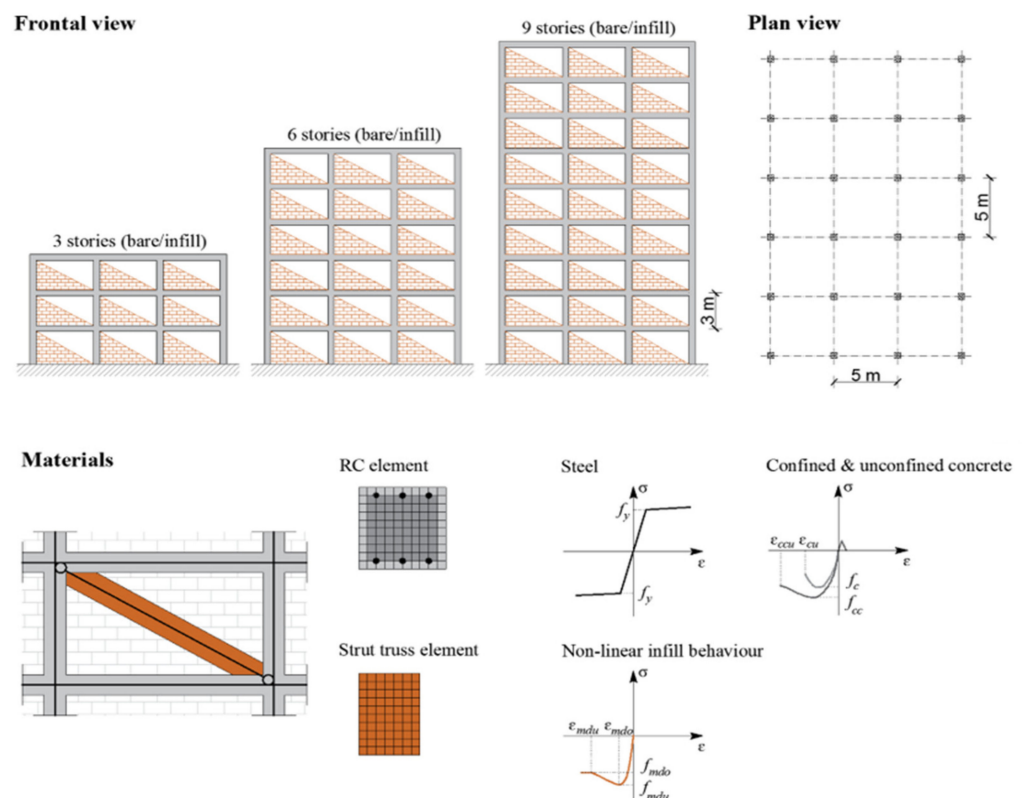


Figure 3. Main geometrical and material characteristics of the analyzed structural archetypes.

The beams and columns are designed considering a C25/30 according to the Italian Building Code [29], with a characteristic compressive strength f_{ck} equal to 25 MPa and a B450C reinforcing steel with characteristic yielding tensile strength f_{yk} equal to 450 MPa. To account for the non-linear material behavior, suitable models are adopted: in detail, Mander et al.'s [30] model *Concrete04* and Menegotto and Pinto's [31] model *Steel02* of materials for core/cover concrete and reinforcement rebars are, respectively, used. Single-

strut truss elements with a non-linear behavior characterized by Di Trapani et al.'s [32] model are adopted to capture the overall stiffening effect caused by the interaction of masonry infills with the RC frame. The masonry compressive strength f_m and the elastic modulus E_m along the two orthogonal directions are assumed to be equal to 7.28 MPa and 7400 MPa for the holes parallel direction, and about 2.4 MPa and 4408 MPa for the direction perpendicular to the load. The masonry infills are characterized by a thickness of 25 cm and distributed over the entire external perimeter of the buildings, whereas the contribution of the staircase to the stiffness of the building is herein neglected. As regards the loading actions, the dead and live loads for the roof are assumed to be equal to 5.5 kN/m² and 0.5 kN/m², whereas their values are fixed at 6.5 kN/m² and 2 kN/m² for the remaining floors. Both the high-ductility class (DCH) and medium-ductility class (DCM) are considered, thus leading to a total of 12 different archetype RC frames resulting from the combination of the different number of stories, ductility class, and presence/absence of masonry infills.

4. Seismic Design and Assessment

The archetype structures are analyzed with the prototype seismic design-assessment software described above.

4.1. Seismic Design

The seismic design is carried out with the classic Response Spectrum Analysis method [33,34], considering only 2D frames, due to the fulfillment of the regularity criteria that allow ignoring 3D effects. For specific irregular structures, ad hoc 3D computations are required, also adopting different formulations able to explicitly account for the main features in terms of the mass and stiffness of the infilled masonry panels [35].

For the seismic design, the first fundamental period T_1 is estimated with the simplified expression suggested by the instructions for the application of the Italian Building Code:

$$T_1 = 0.075H^{3/4} \quad (4)$$

where H is the building height in meters, and then it is possible to derive the elastic spectral acceleration $S_{ae}(T_1)$ starting from the 10% in 50 years exceedance probability UHS.

Some trials are carried out to identify the $S_{ae}(T_1)$ range for the different elevation configurations: the results show how for the Italian context, 3-story archetypes are characterized by a range of $S_{ae}(T_1)$ between 0.1 g and 1 g, whereas the 6- and 9-story archetypes are enclosed in the intervals 0.1–0.75 g and 0.1–0.5 g, respectively. Based on such consideration, the frames' sizing is performed considering an $S_{ae}(T_1)$ resolution equal to 0.05 g.

Hence, for each configuration, the seismic design-assessment tool is launched so that the resulting sizing satisfies the code minimum requirements, and at the same time, tries to optimize the elements' sections without significant oversizing. To this end, Figure 4 shows, as an example, the accuracy of the developed design tool by showing the obtained overstrength factors against the target value required by the Code for one of the investigated layouts.

It can be observed how the variations in the beams' flexural reinforcement and columns' concrete area are directly proportional to the increase in the elastic spectral acceleration, and also how the design tool is able to fulfill the overstrength design limit for ductility design required by the Code.

The resulting sizing is later used in combination with the non-linear material models as input for the automatized construction of the non-linear structural model in the OpenSees environment to carry out pushover analyses. Figures 5 and 6 illustrate the capacity curves resulting from the pushover analyses derived according to [36], respectively, for all the RC bare and infilled archetypes as a function of the increasing $S_{ae}(T_1)$ values.

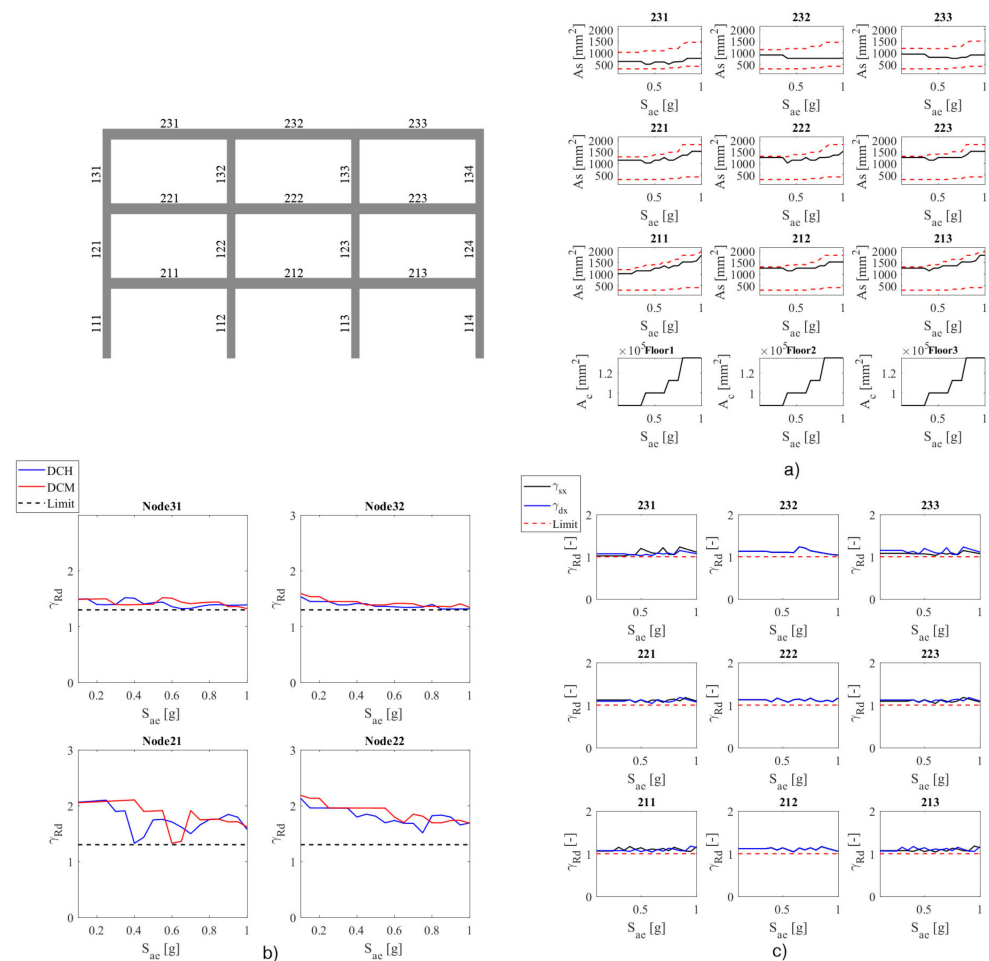


Figure 4. Seismic design outputs for the 3-storey code-conforming configuration: (a) beams' longitudinal reinforcement and columns' section area, (b) nodes' overstrength factors and (c) beams' overstrength factors.

The pushover curves of the code-compliant bare frames show an increase in the base shear proportionally to the elastic spectral acceleration, which proves the goodness of the developed design procedure. Furthermore, the displacement corresponding to the 'yielding point' decreases as the acceleration increases, and this could be ascribed to the greater dimension of the sections, which is related to a higher global stiffness. Moreover, there is no clear discrepancy in terms of the ultimate displacement capacity between the two design ductility classes, given the number of floors. On the contrary, the DCM frames reach a higher base shear than the DCH ones, and this could be based on the fact that the former is designed with a lower value for the behavior factor, which is reflected in a more restrictive design. In addition, looking at the increase in the number of stories, it is possible to observe a slight enhancement in terms of both the ultimate displacement and maximum base shear.

On the other hand, the pushover curves of the infilled frames exhibit a clear increasing in terms of the global stiffness due to the presence of diagonal struts. Thus, there is a clear decrease in the base shear after the attainment of the peak value. As an example, this drop is close to 50% for the 3-storey configurations. However, the capacity curves show the better performance of the DCM configurations in terms of the maximum base shear. In this regard, the adoption of a higher design spectral acceleration due to a lower behavior factor in the DCM leads to frames with sections of greater size that reflect an enhancement of the maximum base shear achievable. There is no significant difference in terms of the ultimate displacement between the two ductility classes. On the contrary, the performance improves according to the number of stories due to the greater flexibility of taller buildings.

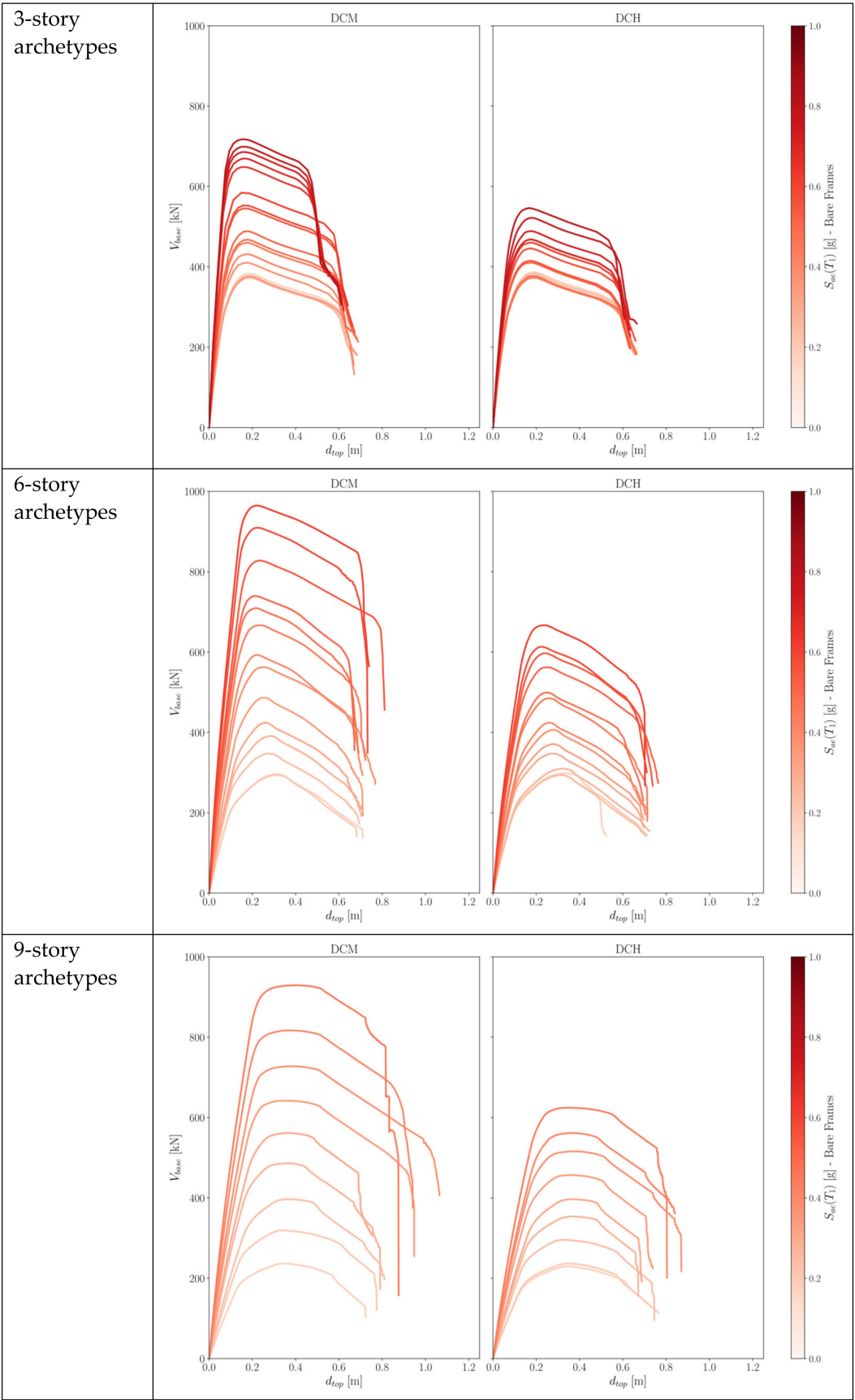


Figure 5. Pushover curves for code-compliant RC bare frames as a function of $S_{ae}(T_1)$.

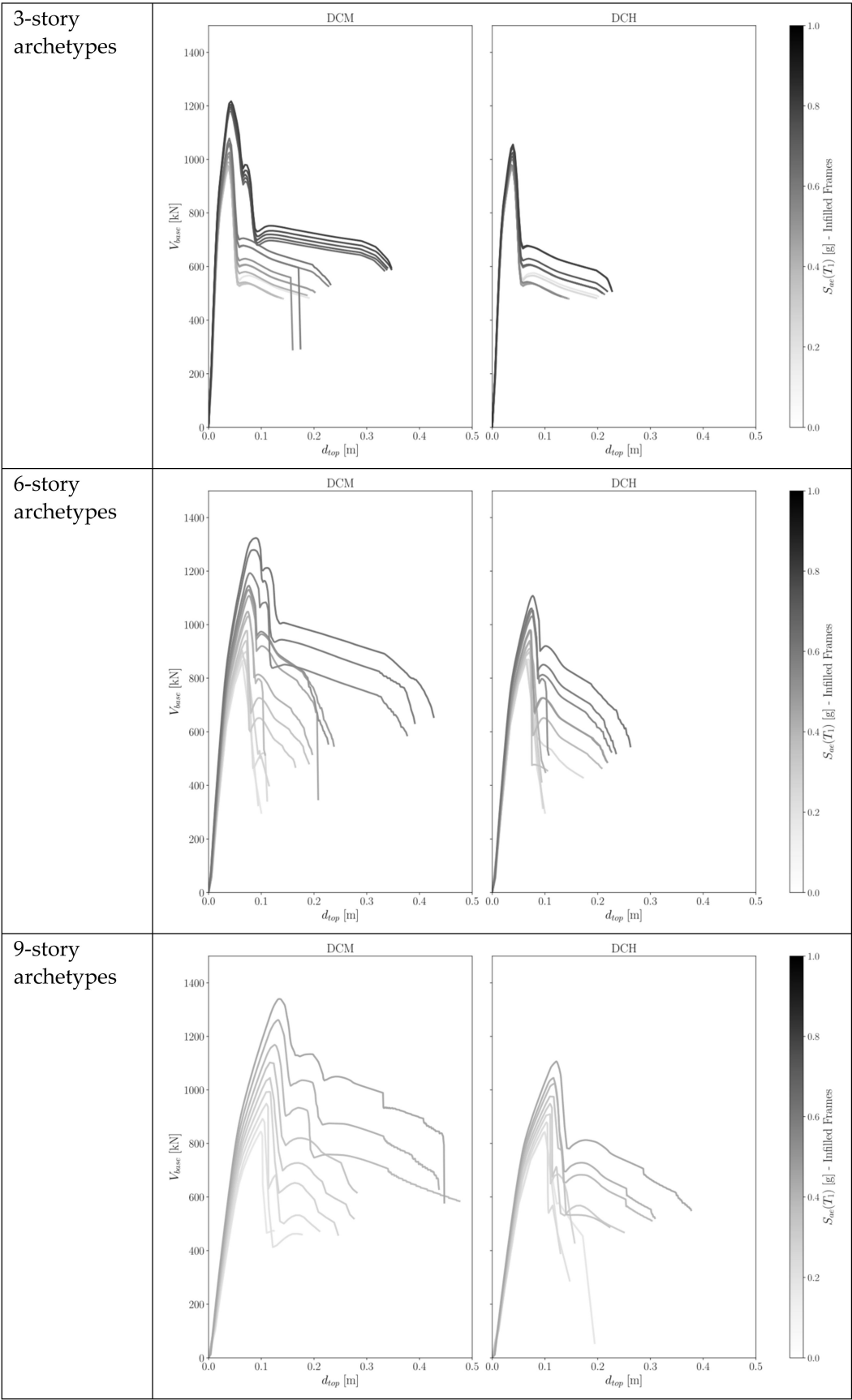


Figure 6. Pushover curves for code-compliant RC infilled frames as a function of $S_{ae}(T_1)$.

4.2. Seismic Fragility Assessment

Capacity curves have been enveloped to obtain the definition of an equivalent SDOF system, which would be adopted to carry out NLTHAs. This choice has been possible due to the global configuration of the prototypes. They meet the regularity requirements in terms of both the plan and elevation, so the torsional effects do not affect their seismic response. However, before describing the idealization procedure, some considerations about this idealization have to be highlighted. First of all, it has to be underlined that in the recent literature, there is an increasing number of studies that attempt to simplify the fragility assessment by making use of a hybrid approach, which entails determining the capacity curve by means of pushover techniques and then evaluating the dynamic response with the use of equivalent SDOFs [26,37,38]. In more depth, a recent publication by Suzuki and Iervolino [37] revealed that the eSDOF system idealization could quite often effectively address the seismic failure rate of the related MDOF building, especially when the regularity criteria are met. Moreover, the eSDOFs were shown to be less prone than 3D models to exhibit the problem of dynamic numerical instability, which is a phenomenon that detrimentally affects the statistical process of deriving fragility curves.

Therefore, the SDOF systems have been characterized by means of a trilinearized backbone starting from the capacity curves of the frames. This strategy has already been widely adopted in the literature [39]; in particular, it has followed the approach contained in [26]. Specifically, the force-displacement behavior has a first elastic portion and a second perfectly plastic branch, which precedes the last linear descending phase. The relevant points have been calibrated using the principle of equal areas between the capacity curves and the idealized one, and then the first modal participation factor Γ has been used to switch from the MDOF system to the SDOF one. As noted in Figure 7, the force at the first and second points is fixed equal to the maximum base shear, while the ‘yield displacement’ is derived by equalizing the area ranging from the initial point to the one mentioned. Hence, the ‘post-capping’ trend is determined similarly. Subsequently, the dynamic behavior of the equivalent SDOF has been recreated with a hysteretic peak-orientated model in the OpenSees environment to be able to perform the vulnerability assessment. Finally, it should be noted that, for simplicity, a damping ζ proportional to the mass matrix has been set.

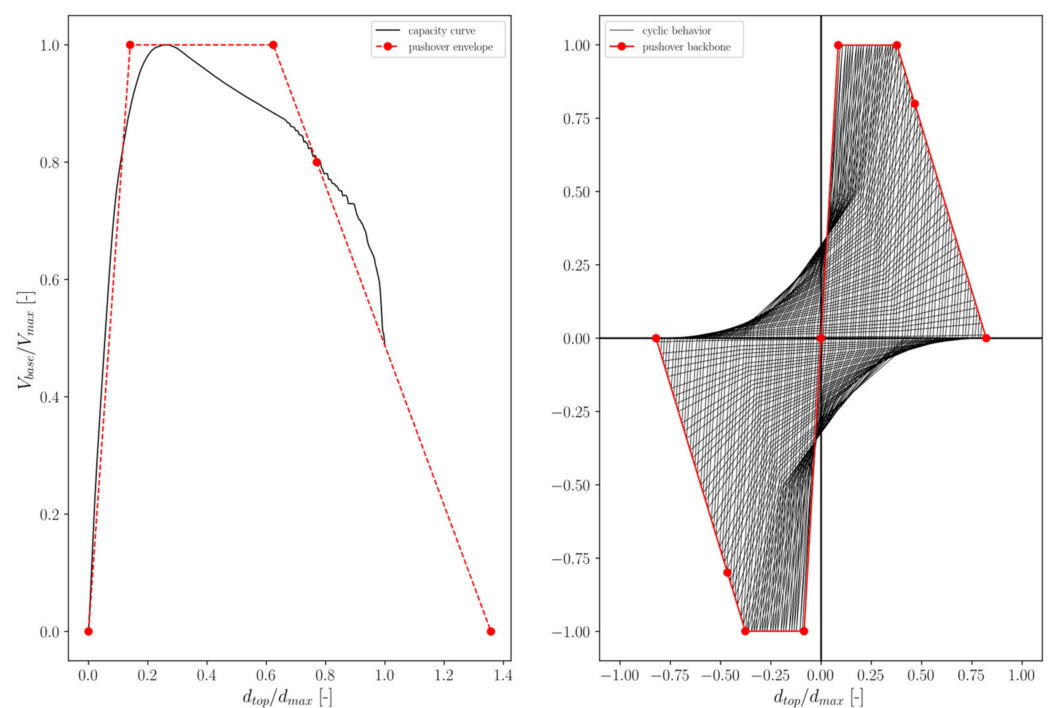


Figure 7. Equivalent SDOF characterization.

The next step in the main framework consists of deriving the fragility curves by means of techniques based on non-linear dynamic analyses, and in particular, the present study applies the so-called Cloud Analysis [40] because it shows the highest effectiveness and flexibility for such a type of analysis. With this method, the system is subjected to a series of unscaled ground motion records N_{GM} , and the maximum response of a structural parameter edp is registered during the analysis. In this way, the fragility curve of a specific damage state DS takes its origin from the linear regression in the logarithmic space of the N_{GM} sample of ground motion intensities im and their respective edp , as illustrated in Section 2. Here, the peak ground acceleration PGA has been picked up as the intensity measure representative of each ground motion, while the displacement of the free node at the top of the equivalent SDOF system stands for the edp parameter.

A dataset containing the ground motion records and the desirable damage states to obtain the fragility curves has been assembled by collecting a group of 200 unscaled records belonging to the 2 horizontal components of 100 different seismic events. This dataset has been built up with an M_w - R_{epi} criterium that is consistent with the seismic disaggregation process. Specifically, a range of variation for the magnitude and epicentral distance has been fixed, and for each step, a series of five events has been collected. However, it should be underlined that increasing the magnitude detrimentally decreases the number of events; thus, for high-intensity events, the selection switched from five to two. Hence, a sample of uniformly spatial events has been obtained, as reported in Figure 8.

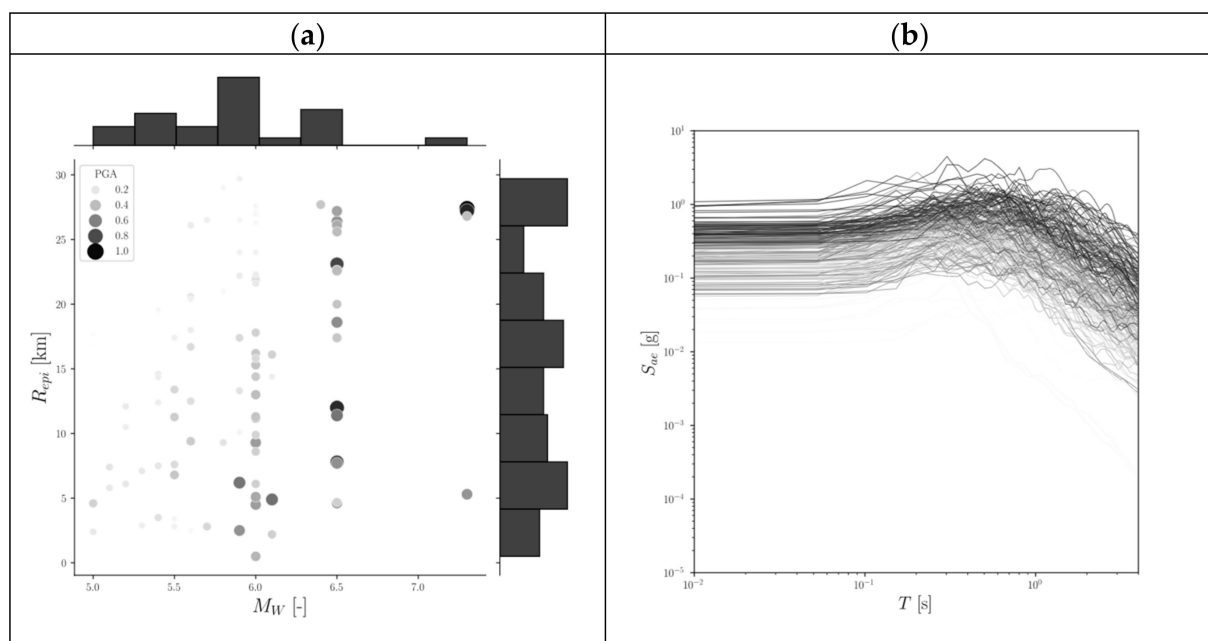


Figure 8. M_w - R_{epi} data (a) and elastic spectra (b) for the dataset of 200 selected events.

The engineering demand parameter considered during the non-linear dynamic analyses to capture the structural response of the equivalent systems has been set in terms of the top displacement since the objective is to account for the flexural behavior of code-conforming frames designed with capacity-design rules. Hence, four relevant damage states have been identified, namely:

- $ds1$ = *Slight Damage (SD)*, which coincides with the displacement where the backbone of the SDOF reaches the elastoplastic branch; thus, this state depicts the yielding of the system;
- $ds2$ = *Moderate Damage (MD)* is reached with the onset of the capping-point displacement;
- $ds3$ = *Near-Collapse Damage (ND)* is located at the attainment of 80% of the maximum base shear in the descending branch of the behavior curve, in compliance with [26];

- $ds4$ = Collapse Damage (CD) occurs at a top displacement corresponding to a base shear approximately 50% of the maximum.

Therefore, all the non-linear dynamic analyses could be performed for each elevation configuration, ductility class, and elastic spectral acceleration $S_{ae}(T_1)$ to obtain the fragility parameters θ and σ for each damage state previously defined. To this end, Figure 9 presents the correlation between the median of the vulnerability θ and the elastic spectral acceleration S_{ae} of a generic construction site.

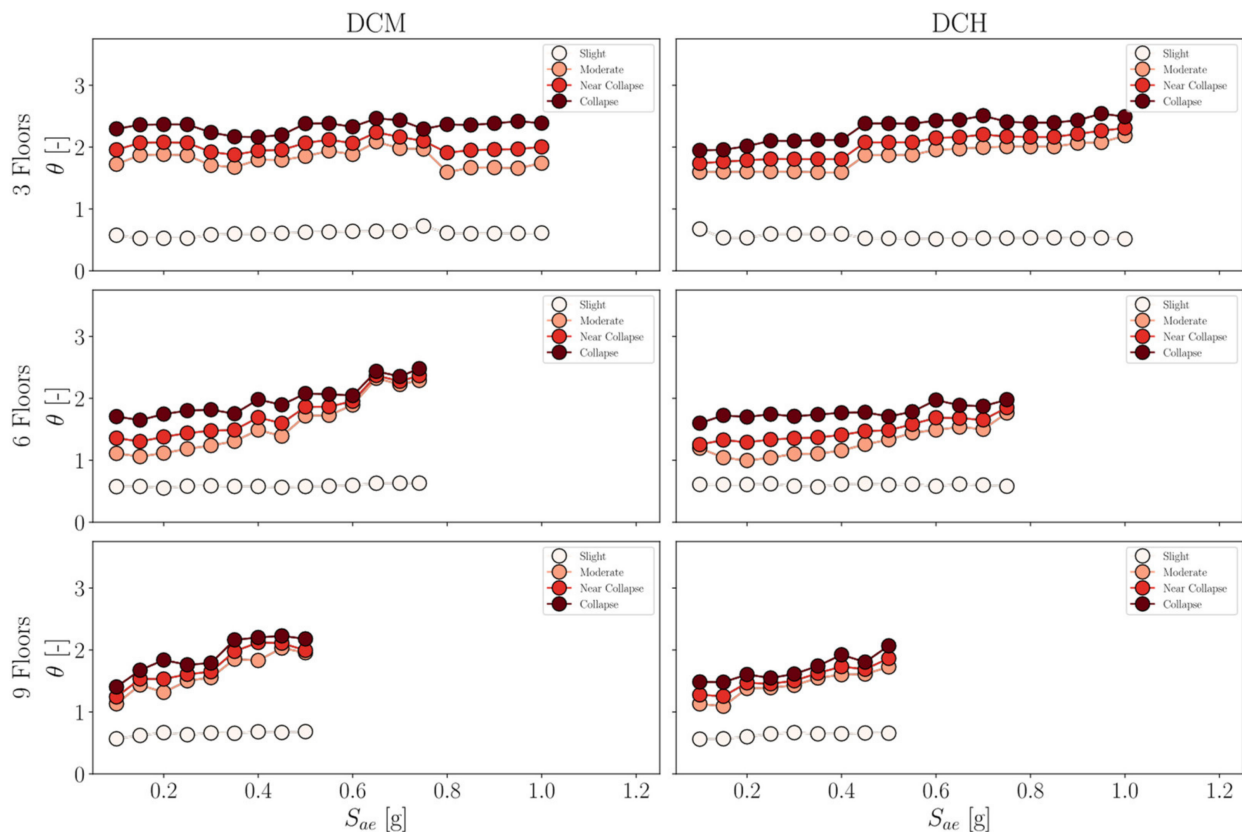


Figure 9. Correlation between the median parameter θ and the spectral acceleration S_{ae} for bare frames.

Hence, this figure indicates that the vulnerability of the frame decreases with an increasing number of floors, given the damage state. Furthermore, the results show no significant differences between the two classes of ductility, as the median values are quite similar for the same elevation configuration. On the contrary, there is a discrepancy in the global trend of the values referring to the variation in the elastic spectral acceleration. At this point, it is possible to derive the seismic fragility curves for each desired damage state. As an example, the curves for the near collapse damage state are reported for both the bare and infilled configurations referring to the near collapse damage state.

The almost steady trend in the median values for the 3-story layouts leads to a strict bundle of curves, while for the other stories, the increasing trend of the median according to the elastic spectral acceleration results in a wider scatter of the fragilities. Thereafter, these results have been compared to those obtained for the bare frames in order to detect how the stiffening of the infills affects the vulnerability. Hence, Figure 10 compares the regions of minimum and maximum fragility between the bare and infilled layouts, referring to the near collapse damage state; thus, the greater vulnerability of the second case is highlighted.

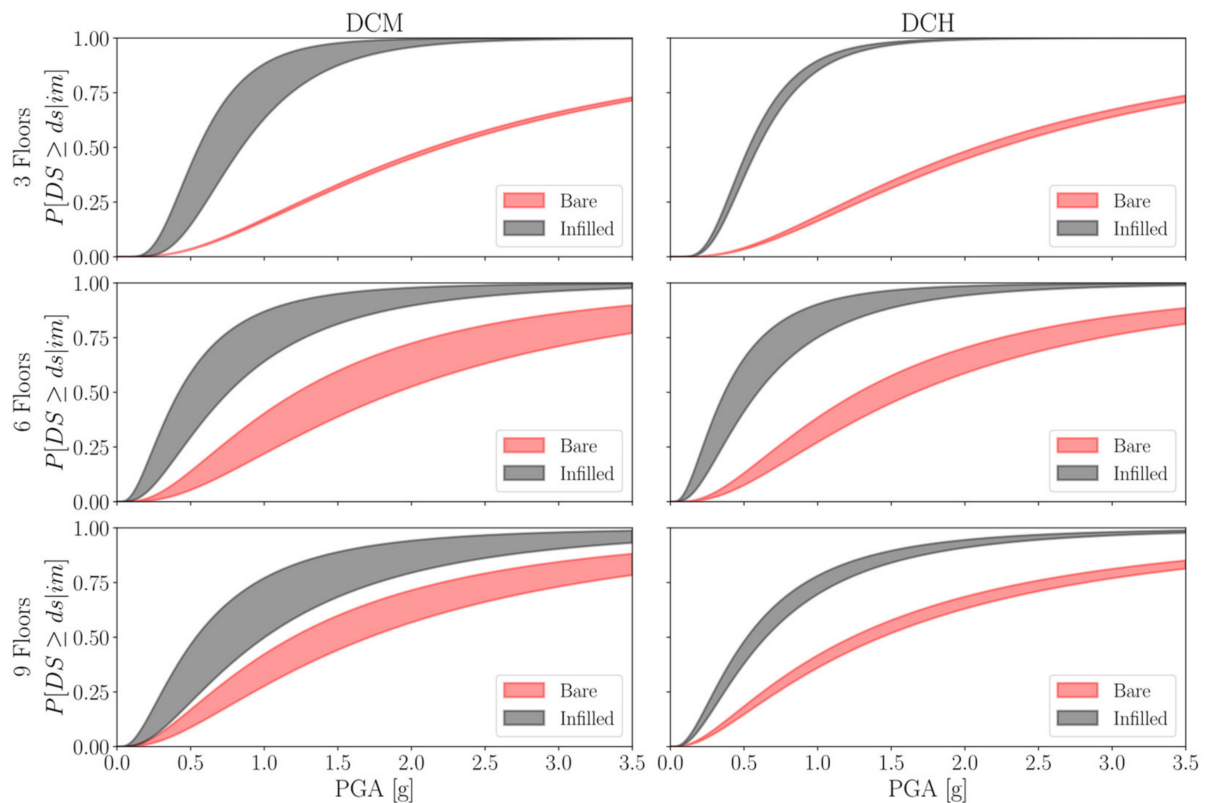


Figure 10. Fragility intervals for the investigated code-compliant bare and infilled layouts.

5. Computation of Code-Compliant Seismic Reliability Maps

The last step in the established procedure aims to evaluate the seismic failure rates of code-compliant RC frames along the Italian territory via the use of the parametric fragility analyses results. A sketch of the required workflow is outlined in Figure 11. In more depth, the 10% in 50 years exceedance probability UHS is first derived from the seismic hazard map currently in force in Italy and used to quantify the elastic spectral acceleration $S_{ae}(T_1)$ based on the first fundamental period T_1 design estimate carried out with Equation (4). In this way, it is possible to establish the level of seismic intensity that would be adopted to design the prototype frames located at the site of interest.

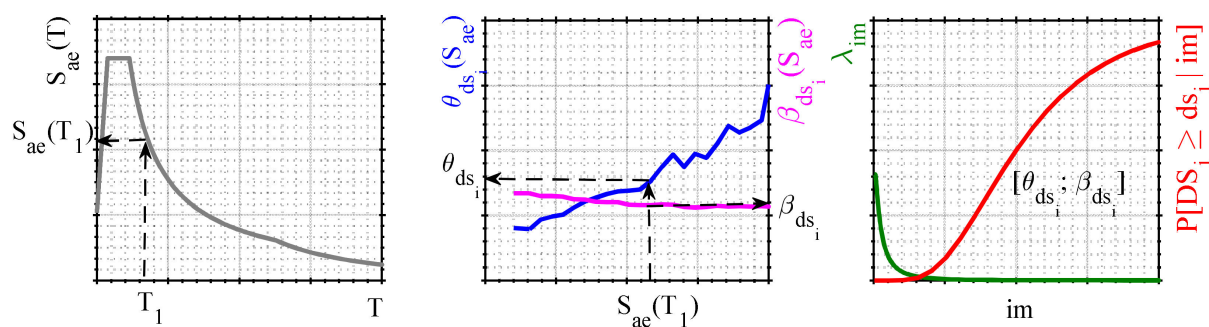


Figure 11. Sketch of the workflow for the code-compliant seismic reliability calculation.

The fragility parameters θ and β are subsequently obtained for each DS of interest. The fragility curves are then computed and later coupled with the seismic hazard curve of the site of interest to obtain the seismic failure rate λ_f accordingly to Equation (2). As regards the seismic hazard, a MATLAB routine is implemented to automatically reproduce code UHSs for a generic site of interest. The UHSs are first computed on soil category A (i.e., rock-like geological formation, including at most 3 m of weaker material at the surface,

with an average shear-wave velocity $V_{S,eq}$ of the upper 30 m higher than 800 m/s) and then amplified with the topographic–stratigraphic amplification coefficient S in accordance with the Italian Building Code [29] for considering the specific soil condition.

Figure 12 plots both the seismic hazard map with a ground acceleration of the 50-year exceedance probability computed at the bedrock and the one determined by assuming the effective soil condition in each site. Hence, this figure outlines the strong effect of considering the soil condition on the spatial distribution of the seismic hazard. For instance, the high amplification factor of soil categories C or D spreads the seismic hazard of the sites in the northeast of Italy in such a way that they reach values of intensity measure similar to those of the well-known locations in the center of Italy.

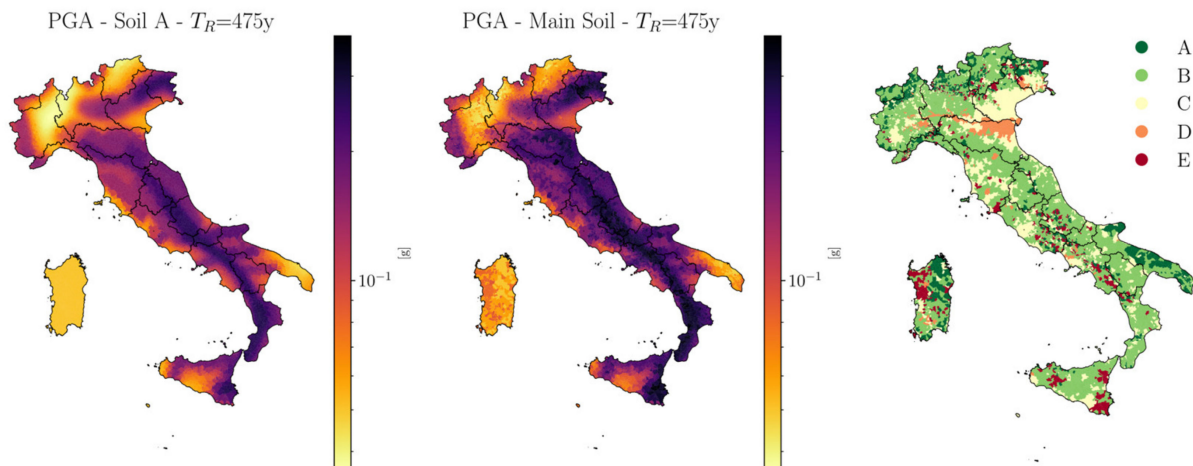


Figure 12. Seismic hazard maps and main soil category.

Hence, the continuous form of the hazard curve is obtained through the interpolation of the amplified ground accelerations corresponding to nine different return periods. To achieve this aim, there are several formulations developed in the literature, such as the closed-form one proposed in [41]. In the present study, a quadratic function in the logarithmic space has been followed, as suggested in [42] for Italy:

$$\lambda_{im}(im) = k_0 e^{[-k_1 \ln(im) - k_2 \ln^2(im)]} \quad (5)$$

where the k_0, k_1, k_2 coefficients are determined by minimizing the interpolation error. Consequently, the code-compliant seismic failure rates are computed by numerically solving the integral (4), coupling the seismic hazard curves with the fragility curves for all the identified damage states. Thus, the results for both the bare and infilled configurations are presented in Figure 13, which shows their range of variation, whereas Figure 14 shows as an example the geographical distribution of the seismic failure rates obtained for all the configurations with respect to the NC damage state. In addition, Tables 1 and 2 report the minimum, the maximum, and the mean values of the seismic failure rates.

A similar global trend is depicted for both the configurations, i.e., the bare and infilled frames. There is an opposite trend between the seismic safety and the number of stories, since the 9-story frames exhibit higher failure rates than the 3-story ones. However, the position of the median marker in Figure 12 is indicative of a skewed distribution, with most of the values located at the upper limit. Moreover, the DCM cases perform slightly better than the DCH cases in the NC and C damage states. This trend could be due to the lower behavior factors of code-compliant buildings adopted in the design process for the DCM class, which seems to better address the seismic safety.

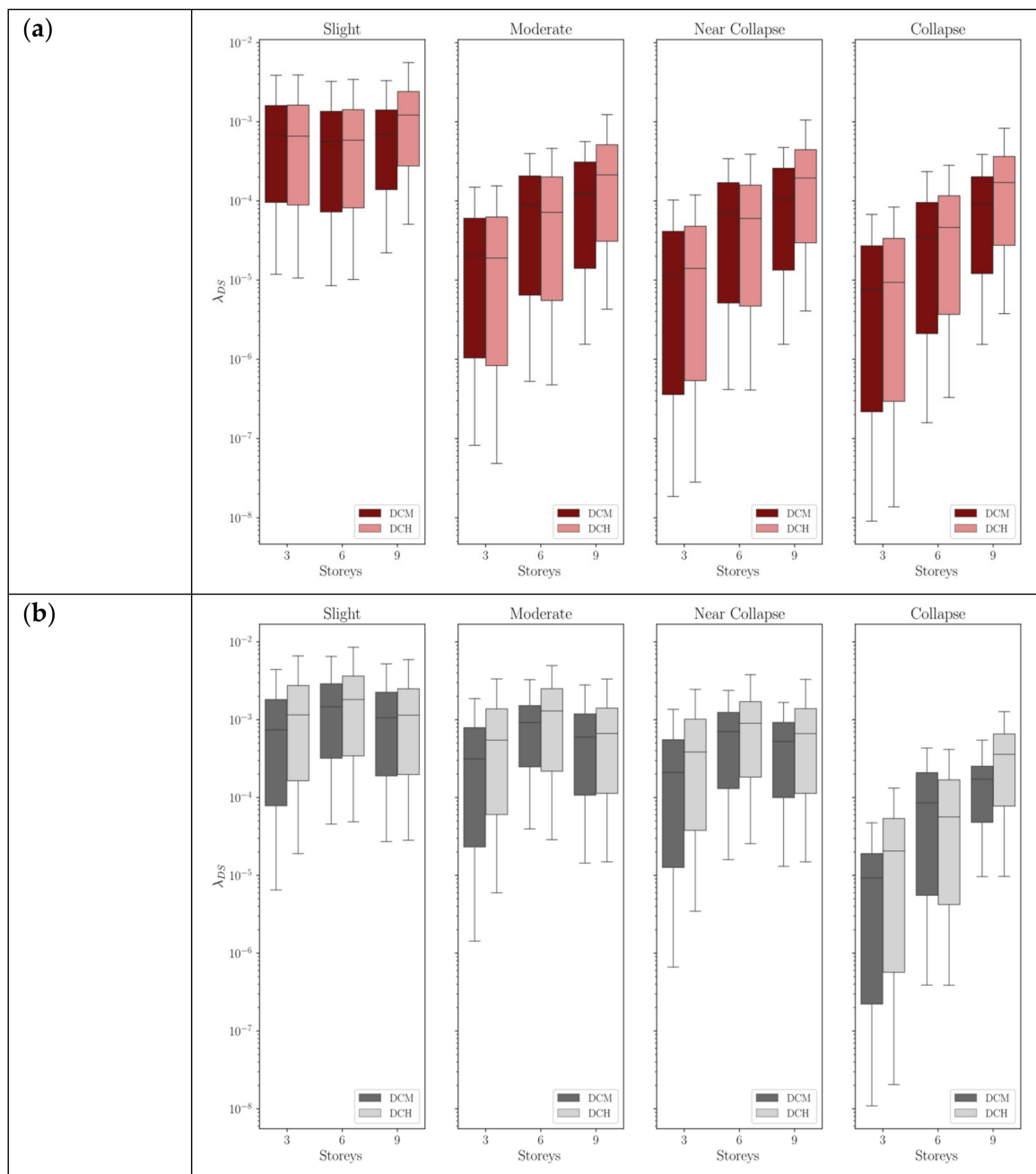


Figure 13. Seismic failure rates boxplot for the (a) bare-frame and (b) infilled-frame configurations.

Lastly, a regression analysis has been carried out on the failure rate data to establish the relationship between the seismic design action on the construction site and the achievable code-conforming seismic reliability. In this way, practitioners could use these laws to obtain a rough estimate of the structural safety when designing a building following the current code provisions. A structure-independent intensity measure has been considered, namely the PGA at the ground level. Hence, the following functional form has been adopted, linking λ_f and PGA at the ground level in terms of [g] due to its statistical significance using the R^2 parameter:

$$\ln(\lambda_f) = k_0 \cdot e^{[k_1 \cdot \ln(PGA) + k_2 \ln^2(PGA)]} + \sigma \varepsilon \quad (6)$$

where ε is a normal random variable with zero mean and unit variance, σ represents the standard deviation of the model error, and k_0 , k_1 and k_2 are the model parameters

calibrated to minimize the interpolation error. The analytical formulation was inspired by the functional form used to fit the seismic hazard curves, given that the numerical results demonstrated how the resulting seismic failure rates for Italian code-conforming RC frame buildings appear strongly correlated with the seismic hazard estimates. Figure 15 shows the seismic failure rate vs. design PGA regression models fitted for the analyzed 3-, 6- and 9-story bare frames, whereas Tables 3 and 4 list the main parameters of the λ_f —the design PGA regression models for both the bare and infilled layouts, respectively.

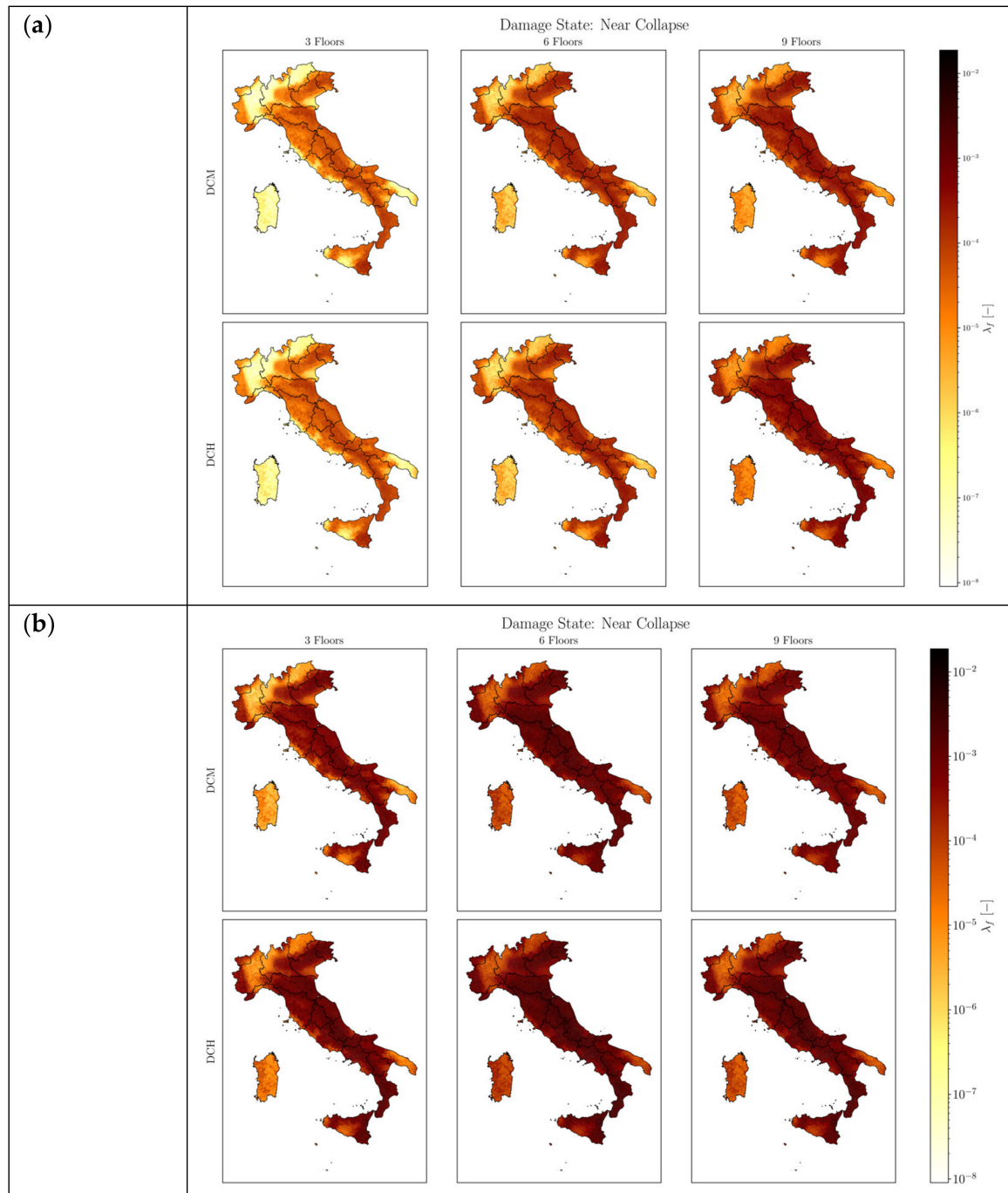


Figure 14. Code-compliant seismic failure rates maps for the near-collapse (NC) damage state: (a) bare frames and (b) infilled frames.

Table 1. Summary of the failure rates—Bare frames.

Case	Damage State	λ_f		
		Min	Max	Mean
3-DCH	ds_1 (SD)	1.06×10^{-5}	5.61×10^{-3}	9.70×10^{-4}
	ds_2 (MD)	4.85×10^{-8}	2.73×10^{-4}	3.74×10^{-5}
	ds_3 (NC)	2.82×10^{-8}	2.36×10^{-4}	2.92×10^{-5}
	ds_4 (C)	1.37×10^{-8}	1.89×10^{-4}	2.10×10^{-5}
3-DCM	ds_1 (SD)	1.18×10^{-5}	5.65×10^{-3}	9.72×10^{-4}
	ds_2 (MD)	8.23×10^{-8}	2.94×10^{-4}	3.75×10^{-5}
	ds_3 (NC)	1.86×10^{-8}	2.28×10^{-4}	2.58×10^{-5}
	ds_4 (C)	9.07×10^{-9}	1.66×10^{-4}	1.72×10^{-5}
6-DCH	ds_1 (SD)	1.02×10^{-5}	4.67×10^{-3}	8.47×10^{-4}
	ds_2 (MD)	4.76×10^{-7}	4.61×10^{-4}	1.13×10^{-4}
	ds_3 (NC)	4.09×10^{-7}	4.03×10^{-4}	9.06×10^{-5}
	ds_4 (C)	3.30×10^{-7}	3.36×10^{-4}	6.76×10^{-5}
6-DCM	ds_1 (SD)	8.49×10^{-6}	3.89×10^{-3}	7.88×10^{-4}
	ds_2 (MD)	5.25×10^{-7}	3.97×10^{-4}	1.13×10^{-4}
	ds_3 (NC)	4.16×10^{-7}	3.42×10^{-4}	9.31×10^{-5}
	ds_4 (C)	1.58×10^{-7}	2.63×10^{-4}	5.38×10^{-5}
9-DCH	ds_1 (SD)	5.07×10^{-5}	6.18×10^{-3}	1.43×10^{-3}
	ds_2 (MD)	4.28×10^{-6}	1.43×10^{-3}	3.02×10^{-4}
	ds_3 (NC)	4.06×10^{-6}	1.13×10^{-3}	2.60×10^{-4}
	ds_4 (C)	3.76×10^{-6}	8.28×10^{-4}	2.13×10^{-4}
9-DCM	ds_1 (SD)	2.21×10^{-5}	4.04×10^{-3}	8.55×10^{-4}
	ds_2 (MD)	1.55×10^{-6}	5.63×10^{-4}	1.68×10^{-4}
	ds_3 (NC)	1.54×10^{-6}	4.74×10^{-4}	1.44×10^{-4}
	ds_4 (C)	1.54×10^{-6}	3.86×10^{-4}	1.16×10^{-4}

Table 2. Summary of the failure rates—Infilled frames.

Case	Damage State	λ_f		
		Min	Max	Mean
3-DCH	ds_1 (SD)	1.90×10^{-5}	8.99×10^{-3}	1.61×10^{-3}
	ds_2 (MD)	5.96×10^{-6}	3.84×10^{-3}	7.75×10^{-4}
	ds_3 (NC)	3.46×10^{-6}	2.64×10^{-3}	5.62×10^{-4}
	ds_4 (C)	2.05×10^{-8}	1.73×10^{-4}	2.90×10^{-5}
3-DCM	ds_1 (SD)	6.49×10^{-6}	5.80×10^{-3}	1.07×10^{-3}
	ds_2 (MD)	1.43×10^{-6}	1.87×10^{-3}	4.55×10^{-4}
	ds_3 (NC)	6.63×10^{-7}	1.36×10^{-3}	3.22×10^{-4}
	ds_4 (C)	1.09×10^{-8}	1.13×10^{-4}	1.22×10^{-5}
6-DCH	ds_1 (SD)	4.88×10^{-5}	9.44×10^{-3}	2.12×10^{-3}
	ds_2 (MD)	2.87×10^{-5}	4.97×10^{-3}	1.40×10^{-3}
	ds_3 (NC)	2.56×10^{-5}	4.11×10^{-3}	1.02×10^{-3}
	ds_4 (C)	3.87×10^{-7}	4.94×10^{-4}	1.00×10^{-4}
6-DCM	ds_1 (SD)	4.56×10^{-5}	8.51×10^{-3}	1.77×10^{-3}
	ds_2 (MD)	3.95×10^{-5}	3.69×10^{-3}	9.63×10^{-4}
	ds_3 (NC)	1.59×10^{-5}	2.38×10^{-3}	7.35×10^{-4}
	ds_4 (C)	3.90×10^{-7}	4.32×10^{-4}	1.17×10^{-4}
9-DCH	ds_1 (SD)	2.82×10^{-5}	7.09×10^{-3}	1.46×10^{-3}
	ds_2 (MD)	1.49×10^{-5}	3.77×10^{-3}	8.33×10^{-4}
	ds_3 (NC)	1.49×10^{-5}	3.61×10^{-3}	8.06×10^{-4}
	ds_4 (C)	9.69×10^{-6}	1.27×10^{-3}	3.82×10^{-4}
9-DCM	ds_1 (SD)	2.71×10^{-5}	6.20×10^{-3}	1.32×10^{-3}
	ds_2 (MD)	1.44×10^{-5}	2.97×10^{-3}	7.06×10^{-4}
	ds_3 (NC)	1.30×10^{-5}	1.66×10^{-3}	5.37×10^{-4}
	ds_4 (C)	9.65×10^{-6}	5.47×10^{-4}	1.67×10^{-4}

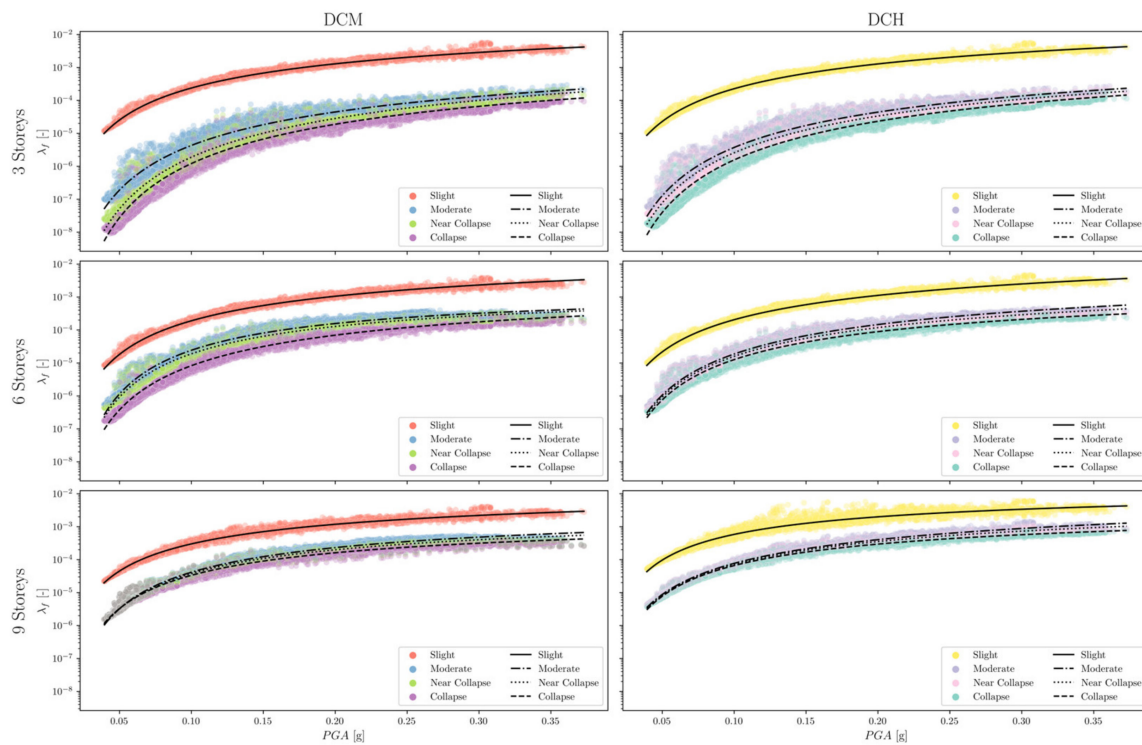


Figure 15. Correlation laws between the peak ground acceleration PGA and the seismic failure rate λ_f for the failure rate estimation.

Table 3. Main parameters of the λ_f —Design PGA regression models for bare frames.

Case	Damage State	k_0	k_1	k_2	σ	R^2
3-DCH	ds_1 (SD)	−4.048	−0.293	0.010	0.124	0.994
	ds_2 (MD)	−6.473	−0.241	0.020	0.337	0.981
	ds_3 (NC)	−6.599	−0.246	0.019	0.369	0.979
	ds_4 (C)	−6.744	−0.257	0.018	0.413	0.976
3-DCM	ds_1 (SD)	−4.105	−0.282	0.011	0.120	0.995
	ds_2 (MD)	−6.541	−0.239	0.016	0.339	0.978
	ds_3 (NC)	−6.439	−0.282	0.013	0.408	0.976
	ds_4 (C)	−6.973	−0.243	0.021	0.451	0.972
6-DCH	ds_1 (SD)	−4.229	−0.275	0.012	0.122	0.994
	ds_2 (MD)	−5.964	−0.203	0.025	0.207	0.990
	ds_3 (NC)	−6.324	−0.175	0.029	0.220	0.988
	ds_4 (C)	−6.792	−0.143	0.034	0.245	0.984
6-DCM	ds_1 (SD)	−4.392	−0.245	0.020	0.125	0.994
	ds_2 (MD)	−7.031	−0.037	0.062	0.255	0.983
	ds_3 (NC)	−6.995	−0.067	0.054	0.257	0.983
	ds_4 (C)	−6.826	−0.155	0.035	0.287	0.982
9-DCH	ds_1 (SD)	−4.707	−0.113	0.037	0.128	0.974
	ds_2 (MD)	−5.299	−0.217	0.015	0.181	0.994
	ds_3 (NC)	−5.684	−0.171	0.023	0.170	0.994
	ds_4 (C)	−6.208	−0.114	0.033	0.172	0.993
9-DCM	ds_1 (SD)	−4.838	−0.164	0.026	0.122	0.991
	ds_2 (MD)	−6.297	−0.112	0.040	0.207	0.989
	ds_3 (NC)	−6.543	−0.100	0.040	0.220	0.990
	ds_4 (C)	−6.860	−0.088	0.039	0.245	0.988

Table 4. Main parameters of the λ_f —Design PGA regression models for infilled frames.

Case	Damage State	k_0	k_1	k_2	σ	R^2
3-DCH	ds_1 (SD)	−3.793	−0.266	0.020	0.126	0.994
	ds_2 (MD)	−4.449	−0.223	0.029	0.138	0.994
	ds_3 (NC)	−4.684	−0.218	0.030	0.155	0.993
	ds_4 (C)	−8.426	0.009	0.079	0.515	0.960
3-DCM	ds_1 (SD)	−4.104	−0.241	0.030	0.146	0.994
	ds_2 (MD)	−4.925	−0.187	0.041	0.216	0.989
	ds_3 (NC)	−5.063	−0.205	0.038	0.258	0.986
	ds_4 (C)	−9.765	0.055	0.082	0.745	0.916
6-DCH	ds_1 (SD)	−4.219	−0.129	0.044	0.146	0.989
	ds_2 (MD)	−5.115	−0.011	0.068	0.172	0.985
	ds_3 (NC)	−5.258	−0.050	0.053	0.125	0.991
	ds_4 (C)	−5.739	−0.263	0.010	0.263	0.983
6-DCM	ds_1 (SD)	−4.344	−0.142	0.037	0.126	0.991
	ds_2 (MD)	−5.958	0.041	0.064	0.160	0.979
	ds_3 (NC)	−6.611	0.128	0.092	0.191	0.980
	ds_4 (C)	−6.722	−0.073	0.057	0.287	0.981
9-DCH	ds_1 (SD)	−4.163	−0.207	0.026	0.142	0.990
	ds_2 (MD)	−4.867	−0.148	0.035	0.120	0.993
	ds_3 (NC)	−5.045	−0.119	0.041	0.128	0.992
	ds_4 (C)	−8.350	0.247	0.112	0.261	0.959
9-DCM	ds_1 (SD)	−4.394	−0.175	0.031	0.135	0.991
	ds_2 (MD)	−5.290	−0.097	0.043	0.121	0.993
	ds_3 (NC)	−7.085	0.142	0.092	0.204	0.976
	ds_4 (C)	−8.167	0.074	0.055	0.300	0.907

6. Conclusions

In this work, an extensive numerical simulation has been carried out to assess the seismic reliability implicitly achievable for new reinforced concrete frame constructions designed in accordance with the current technical standards. For this purpose, a general framework has been conceived and implemented in the MATLAB and OpenSees environments to perform thousands of NLTHAs and obtain first the fragility curve sets and then the failure rate estimates for a wide set of layouts characterized by the compliance of the code plan and elevation regularity criteria. The results highlighted how the current design approach based on the definition of seismic actions with a uniform exceedance probability clearly fails to ensure a constant seismic safety, with the seismic failure rates varying up to four orders of magnitude. At the same time, the role of masonry infills has also been clearly outlined in terms of the increase in the failure rate estimates. The results highlighted how the seismic failure rates increase for the higher building layouts, whereas the use of the DCH strategy is not so relevant for achieving a better result in terms of the seismic failure rate with respect to the DCM one. In detail, code-compliant Italian RC bare archetypes are characterized by seismic failure rates ranging from 8.49×10^{-6} to 6.18×10^{-3} for ds_1 , whereas for the ds_2 , ds_3 and ds_4 damage states, the reference intervals are 4.85×10^{-8} – 5.63×10^{-4} , 1.86×10^{-8} – 1.13×10^{-3} , and 9.07×10^{-9} – 8.28×10^{-4} , respectively. Code-compliant Italian RC infilled archetypes are instead characterized by seismic failure rates ranging from 6.49×10^{-6} to 9.44×10^{-3} for ds_1 , whereas for the ds_2 , ds_3 and ds_4 damage states, the reference intervals are 1.43×10^{-6} – 4.97×10^{-3} , 6.63×10^{-7} – 4.97×10^{-3} , and 1.09×10^{-8} – 1.27×10^{-3} , respectively.

On this basis, such outcomes have been used to develop a set of regression models that can be quickly used to relate the 10% exceedance probability in 50 years PGA to the seismic failure rate with respect to different damage states to obtain a preliminary estimate of the seismic safety achievable with a design compliant with the current code prescriptions. The proposed methodology can be used for further investigations aimed at analyzing different

building archetypes as well as deriving regression relationships between different damage states and earthquake intensity measures. Future developments of the present work will be oriented toward introducing some corrective coefficients into the design workflow able to explicitly control the resulting failure probability and fulfilling target reliability levels.

Author Contributions: Conceptualization, G.F. and M.A.Z.; methodology, G.F., L.H. and M.A.Z.; software, G.F.; validation, L.H. and M.A.Z.; formal analysis, G.F. and M.A.Z.; data curation, G.F. and L.H.; writing—original draft preparation, G.F. and M.A.Z.; writing—review and editing, M.A.Z.; supervision, M.A.Z. All authors have read and agreed to the published version of the manuscript.

Funding: This research received no external funding.

Data Availability Statement: Dataset available on request from the authors.

Conflicts of Interest: The authors declare no conflicts of interest.

References

- O'Reilly, G.J.; Calvi, G.M. Conceptual seismic design in performance-based earthquake engineering. *Earthq. Eng. Struct. Dyn.* **2018**, *48*, 389–411. [\[CrossRef\]](#)
- McGuire, R.K. Probabilistic seismic hazard analysis: Early history. *Earthq. Eng. Struct. Dyn.* **2007**, *37*, 329–338. [\[CrossRef\]](#)
- Eurocode 0: Basis of Structural Design*; Structural Eurocodes; European Commission: Brussels, Belgium, 2002.
- Cornell, C.; Krawinkler, H. Progress and challenges in seismic performance assessment. *PEERCenter News* **2000**, *3*, 1–3.
- Bradley, B.A. Design Seismic Demands from Seismic Response Analyses: A Probability-Based Approach. *Earthq. Spectra* **2011**, *27*, 213–224. [\[CrossRef\]](#)
- Faleschini, F.; Zanini, M.A.; Toska, K. Seismic reliability assessment of code-conforming reinforced concrete buildings made with electric arc furnace slag aggregates. *Eng. Struct.* **2019**, *195*, 324–339. [\[CrossRef\]](#)
- Cardone, D.; Conte, N.; Dall'Asta, A.; Di Cesare, A. RINTC project: Nonlinear analyses of Italian code-conforming base-isolated buildings for risk of collapse assessment. In Proceedings of the COMPDYN 2017—Proceedings of the 6th International Conference on Computational Methods in Structural Dynamics and Earthquake Engineering, Rhodes Island, Greece, 15–17 June 2017.
- Camata, G.; Celano, F.; De Risi, M.; Franchin, P.; Magliulo, G.; Manfredi, V.; Masi, A.; Mollaioli, F.; Noto, F.; Ricci, P.; et al. RINTC project: Nonlinear dynamic analysis of Italian code-conforming reinforced concrete buildings for risk of collapse assessment. In Proceedings of the COMPDYN 2017—Proceedings of the 6th International Conference on Computational Methods in Structural Dynamics and Earthquake Engineering, Rhodes Island, Greece, 15–17 June 2017.
- Scozzese, F.; Terracciano, G.; Zona, A.; Della Corte, G.; Dall'Asta, A.; Landolfo, R. RINTC Project: Nonlinear dynamic analysis of Italian code-conforming steel single-storey buildings for collapse risk assessment. In Proceedings of the COMPDYN 2017—Proceedings of the 6th International Conference on Computational Methods in Structural Dynamics and Earthquake Engineering, Rhodes Island, Greece, 15–17 June 2017.
- Camilletti, D.; Cattari, S.; Lagomarsino, S.; Bonaldo, D.; Guidi, G.; Bracchi, S.; Galasco, A.; Magenes, G.; Manzini, C.; Penna, A.; et al. RINTC Project: Nonlinear dynamic analysis of Italian code-conforming URM buildings for collapse risk assessment. In Proceedings of the COMPDYN 2017—Proceedings of the 6th International Conference on Computational Methods in Structural Dynamics and Earthquake Engineering, Rhodes Island, Greece, 15–17 June 2017.
- Goulet, C.A.; Haselton, C.B.; Mitrani-Reiser, J.; Beck, J.L.; Deierlein, G.G.; Porter, K.A.; Stewart, J.P. Evaluation of the seismic performance of a code-conforming reinforced-concrete frame building from seismic hazard to collapse safety and economic losses. *Earthq. Eng. Struct. Dyn.* **2007**, *36*, 1973–1997. [\[CrossRef\]](#)
- Williams, R.J.; Gardoni, P.; Bracci, J.M. Decision analysis for seismic retrofit of structures. *Struct. Saf.* **2009**, *31*, 188–196. [\[CrossRef\]](#)
- Jeong, S.-H.; Mwafy, A.M.; Elnashai, A.S. Probabilistic seismic performance assessment of code-compliant multi-story RC buildings. *Eng. Struct.* **2012**, *34*, 527–537. [\[CrossRef\]](#)
- Terzic, V.; Mahin, S.A. Using PBEE to assess and improve performance of different structural systems for low-rise steel buildings. *Int. J. Saf. Secur. Eng.* **2017**, *7*, 532–544. [\[CrossRef\]](#)
- Rizwan, M.; Ahmad, N.; Khan, A.N. Seismic Performance of Compliant and Non-Compliant Special Moment-Resisting Reinforced Concrete Frames. *ACI Struct. J.* **2018**, *115*, 1063. [\[CrossRef\]](#)
- Sattar, S. Evaluating the consistency between prescriptive and performance-based seismic design approaches for reinforced concrete moment frame buildings. *Eng. Struct.* **2018**, *174*, 919–931. [\[CrossRef\]](#)
- Harris, J.; Speicher, M. Assessment of Performance-Based Seismic Design Methods in ASCE 41 for New Steel Buildings: Special Moment Frames. *Earthq. Spectra* **2018**, *34*, 977–999. [\[CrossRef\]](#) [\[PubMed\]](#)
- FEMA P-58-5; Seismic Performance Assessment of Buildings, Volume 5: Expected Seismic Performance of Code-Conforming Buildings*. FEMA: Washington, DC, USA, 2018.
- Iervolino, I.; Spillatura, A.; Bazzurro, P. Seismic Reliability of Code-Conforming Italian Buildings. *J. Earthq. Eng.* **2018**, *22*, 5–27. [\[CrossRef\]](#)

20. Silva, V.; Crowley, H.; Bazzurro, P. Exploring Risk-Targeted Hazard Maps for Europe. *Earthq. Spectra* **2016**, *32*, 1165–1186. [CrossRef]
21. Gkimprixis, A.; Tubaldi, E.; Douglas, J. Comparison of methods to develop risk-targeted seismic design maps. *Bull. Earthq. Eng.* **2019**, *17*, 3727–3752. [CrossRef]
22. Luco, N.; Ellingwood, B.; Hamburger, R.; Hooper, J. Risk-Targeted versus Current Seismic Design Maps for the Conterminous United States. In Proceedings of the SEAOC 2007 Convention Proceedings, Squaw Creek, CA, USA, 26–29 September 2007.
23. Zanini, M.A.; Feltrin, G. *Proceedings of the 1st Conference of the European Association on Quality Control of Bridges and Structures, Padua, Italy, 29 August–1 September 2021*; Springer International Publishing: Cham, Switzerland, 2021; pp. 1397–1404.
24. The MathWorks, Inc. MATLAB Version: 9.13.0 (R2022b). 2022. Available online: <https://www.mathworks.com> (accessed on 26 May 2024).
25. McKenna, F.; Scott, M.H.; Fenves, G.L. Nonlinear Finite-Element Analysis Software Architecture Using Object Composition. *J. Comput. Civ. Eng.* **2010**, *24*, 95–107. [CrossRef]
26. Kotic, M.; Fajfar, P.; Dolšek, M. Approximate seismic risk assessment of building structures with explicit consideration of uncertainties. *Earthq. Eng. Struct. Dyn.* **2014**, *43*, 1483–1502. [CrossRef]
27. Cornell, C.A. Engineering seismic risk analysis. *Bull. Seismol. Soc. Am.* **1968**, *58*, 1583–1606. [CrossRef]
28. Cornell, C.A.; Jalayer, F.; Hamburger, R.O.; Foutch, D.A. Probabilistic Basis for 2000 SAC Federal Emergency Management Agency Steel Moment Frame Guidelines. *J. Struct. Eng.* **2002**, *128*, 526–533. [CrossRef]
29. *Aggiornamento Delle “Norme Tecniche per le Costruzioni”*; Gazzetta Ufficiale: Rome, Italy, 2018.
30. Mander, J.B.; Priestley, M.J.N.; Park, R. Theoretical Stress-Strain Model for Confined Concrete. *J. Struct. Eng.* **1988**, *114*, 1804–1826. [CrossRef]
31. Menegotto, M.; Pinto, P.E. Method of analysis for cyclically loaded R.C. plane frames including changes in geometry and non-elastic behaviour of elements under combined normal force and bending. In *IABSE Symp. on Resistance and Ultimate Deformability of Structures Acted on by Well Defined Repeated Loads*; IABSE: Zurich, Switzerland, 1973; pp. 15–22.
32. Di Trapani, F.; Bertagnoli, G.; Ferrotto, M.F.; Gino, D. Empirical Equations for the Direct Definition of Stress-Strain Laws for Fiber-Section-Based Macromodeling of Infilled Frames. *J. Eng. Mech.* **2018**, *144*, 1–17. [CrossRef]
33. *Eurocode 2: Design of Concrete Structures; Part 1-1: General Rules and Rules for Buildings*; European Commission: Brussels, Belgium, 2004.
34. *Eurocode 8: Design of Structures for Earthquake Resistance; Part 1: General Rules, Seismic Actions and Rules for Buildings*; European Commission: Brussels, Belgium, 2004.
35. Ruggieri, S.; Fiore, A.; Uva, G. A new approach to predict the fundamental period of vibration for newly-designed reinforced concrete buildings. *J. Earthq. Eng.* **2021**, *26*, 6943–6968. [CrossRef]
36. Žižmond, J.; Dolšek, M. Formulation of risk-targeted seismic action for the force-based seismic design of structures. *Earthq. Eng. Struct. Dyn.* **2019**, *48*, 1406–1428. [CrossRef]
37. Suzuki, A.; Iervolino, I. Seismic Fragility of Code-conforming Italian Buildings Based on SDOF Approximation. *J. Earthq. Eng.* **2019**, *25*, 2873–2907. [CrossRef]
38. D’Ayala, D.; Meslem, A.; Vamvatsikos, D.; Porter, K.; Rossetto, T.; Crowley, H.; Silva, V. *Guidelines for Analytical Vulnerability Assessment of Low/Mid-Rise Buildings*; Global Earthquake Model: New York, NY, USA, 2014.
39. De Luca, F.; Vamvatsikos, D.; Iervolino, I. Near-optimal piecewise linear fits of static pushover capacity curves for equivalent SDOF analysis. *Earthq. Eng. Amp Struct. Dyn.* **2012**, *42*, 523–543. [CrossRef]
40. Jalayer, F. Direct Probabilistic Seismic Analysis: Implementing Non-Linear Dynamic Assessments. Ph.D. Thesis, Stanford University, Stanford, CA, USA, 2003.
41. Kumar, R.; Gardoni, P. Second-order Logarithmic formulation for hazard curves and closed-form approximation to annual failure probability. *Struct. Saf.* **2013**, *45*, 18–23. [CrossRef]
42. National Research Council of Italy. Guidelines for the Seismic Reliability Assessment for Existing Buildings—CNR-DT 212/2013; 2014. Available online: <https://www.airesingegneria.it/en/archives/italian-technical-standard/guidelines-and-technical-instructions-by-the-national-research-council-of-italy-cnr/cnr-dt-212-2013/> (accessed on 17 April 2024).

Disclaimer/Publisher’s Note: The statements, opinions and data contained in all publications are solely those of the individual author(s) and contributor(s) and not of MDPI and/or the editor(s). MDPI and/or the editor(s) disclaim responsibility for any injury to people or property resulting from any ideas, methods, instructions or products referred to in the content.